Surface recombinations in III-nitride micro-LEDs probed by photon-correlation cathodoluminescence

Sylvain Finot, Corentin Le Maoult, Etienne Gheeraert, David Vaufrey, Gwenolé Jacopin

Surface recombinations in III-nitride micro-LEDs probed by photon-correlation cathodoluminescence

Sylvain Finot,[†] Corentin Le Maoult,[‡] Etienne Gheeraert,[†] David Vaufrey,[‡] and Gwénolé Jacopin[*,†]

[†]*Univ. Grenoble Alpes, CNRS, Grenoble INP*, Institut Néel, 38000 Grenoble, France*
[‡]*Univ. Grenoble Alpes, CEA, LETI, F-38000 Grenoble, France*

E-mail: gwenole.jacopin@neel.cnrs.fr

Abstract

III-nitride micro-LEDs are promising building blocks for the next generation of high performance micro-displays. To reach a high pixel density, it is desired to achieve micro-LEDs with lateral dimensions below 10 µm. With such pixel downscaling, sidewall effects are becoming important and an understanding of the impact of non-radiative surface recombinations is of vital importance. It is thus required to develop an adapted metric to evaluate the impact of these surface recombinations with a nanoscale spatial resolution. Here, we propose a methodology to quantitatively assess the influence of surface recombinations on the optical properties of InGaN/GaN quantum wells based on spatially-resolved time-correlated cathodoluminescence spectroscopy. By coupling this technique to a simple diffusion model, we confirm that the combination of KOH treatment and Al_2O_3 passivation layer drastically reduces surface recombinations. These findings emphasize the need for nanoscale time-resolved experiments to quantify the local changes in internal quantum efficiency of micro-devices.

After more than 30 years of development, III-nitride-based light emitting devices (LEDs) are now widely used for general lighting. Thanks to their high efficiency, this technology is now considered as a promising candidate for µLED display applications. However, the size reduction brings various challenges that are currently preventing their commercialization. In particular, as the surface-to-volume ratio increases, non-radiative surface recombinations at the sidewalls become significant, which limit the efficiency of µLEDs.[1] To mitigate such effects, different passivation techniques have been proposed such as thermal annealing,[2] chemical treatment[3–5] and oxide deposition.[5,6]

Due to the reduced dimensions of such µLEDs, dedicated optical characterization techniques have been specifically implemented. First, the optical properties have been probed by micro-photoluminescence (µ-PL),[3,7] and electroluminescence (EL) spectroscopies.[1,2,8] In addition, cathodoluminescence (CL) spectroscopy has been used to study precisely the edge effects with an excellent spatial resolution.[9] However, if these techniques are well suited to characterize the variation in external quantum efficiency (EQE), they do not allow to disentangle changes in internal quantum efficiency (IQE), light extraction efficiency (LEE) or injection efficiency (IE). Thus, to directly estimate the influence of size reduction on Shockley-Read-Hall recombinations and to be only sensitive to IQE variation, time-resolved photoluminescence (TR-PL) spectroscopy[1,10] have been employed. The spatial resolution of such technique, however, does not allow to

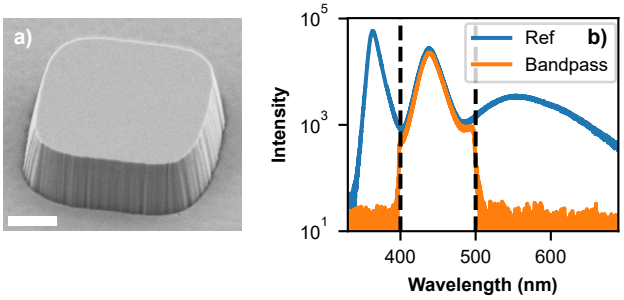

Figure 1: (a) Bird's-eye view SEM image of a $4 \times 4\,\mu m^2$ LED after ICP dry etching and hard mask removal. The scale bar is 1-µm long. (b) CL spectra obtained at 10 kV with and without bandpass filter ($\lambda = 450 \pm 50$ nm).

directly quantify the surface recombination velocity.

Therefore, there is a need for a characterization technique that combines both high spatial and high temporal resolution, in order to assess the changes in IQE induced by the sidewalls without being influenced by changes in injection[11] or light extraction efficiency.[8,12,13]

In this paper, we studied the optical properties of InGaN/GaN MQW µLEDs grown by metal-organic chemical vapor deposition (MOCVD). First, depth-dependent CL spectroscopy is presented to emphasize the importance of possible artefacts of standard CL spectroscopy. Then, thanks to a spatially resolved time-correlated CL setup (SRTC-CL),[14] we probe the carrier lifetime in a InGaN/GaN multiple quantum wells (MQW) near a mesa edge with a spatial resolution of 100 nm and a time resolution better than 50 ps. This enabled us to quantify the impact of surface recombinations on a single µLED with a nanoscale resolution. Finally, the robustness of this technique is demonstrated by comparing samples with different surface treatments.

The InGaN/GaN MQW LED structure was commercially grown on *c*-plane GaN-on-sapphire template. The LED stack consists of a 2 µm-thick *n*-GaN, followed by an $In_{0.15}Ga_{0.85}N$/GaN MQW active region emitting around 440 nm. The *p*-type region consists of a 20-nm thick $Al_{0.15}Ga_{0.85}N$ electron blocking layer (EBL) and 180-nm thick *p*-GaN cap. To define the µLED mesa, 1 µm of SiO_2 has been deposited to be used as a hard mask. Squared mesas with lateral sizes ranging from 2 to 100 µm have been then defined by inductively coupled Cl_2/Ar plasma (ICP) etching. A typical SEM image of a $4 \times 4\,\mu m^2$ LED after dry etching is depicted in Figure 1 (a).

We first probed the optical properties by CL spectroscopy at 10 kV and room temperature. A CL spectrum obtained from a region containing both the mesa and the etched area is displayed in Figure 1 (b). Three spectral regions could be identified. First, the GaN near band edge emission (NBE) is located around 363 nm. Then, the CL contribution centered at 440 nm is attributed to the InGaN/GaN active region. Finally, the broad luminescent band emitting between 500 and 600 nm is ascribed to the GaN defect band (Yellow band).[15] These assignments are further confirmed by the fact that the GaN NBE and YL mainly arise from the etched region while the MQW CL comes from the mesa itself. To ensure to probe mainly the luminescence originating from the active region, a bandpass filter ($\lambda = 450 \pm 50$ nm) is then used, corresponding to the spectral range within which the MQW emission occurs.

In CL spectroscopy, the incident electron energy defines the interaction volume. This interaction volume not only sets the penetration depth but also limits the spatial resolution. In order to study the luminescence of the active region, a substantial number of electrons must overcome the EBL. There is therefore a trade-off between spatial resolution and the MQW luminescence intensity. In Figure 2 (a)-(d), normalized CL images at the MQW energy are shown for different acceleration voltages. Below 7 kV, most of the MQW CL intensity originates from the mesa edges. Indeed, in the center of the mesa, the EBL prevents the carriers generated in the *p*-GaN to diffuse to the MQW region. On the other hand, when the electron beam reaches the sidewalls which deviate by 8° from the vertical, it becomes possible to directly inject carriers into the active region (see the inset of Figure 2 (e)) and thus to collect the MQW CL signal from the edges.

By increasing the acceleration voltage, the penetration depth of the primary electrons in-

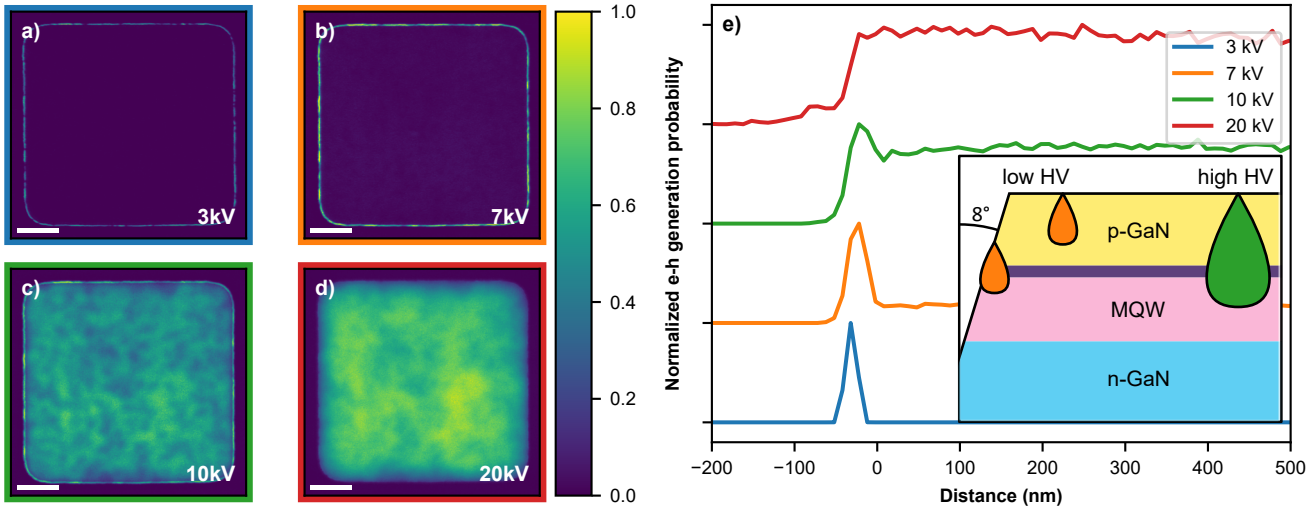

Figure 2: (a)-(d) CL images of the same pixel at the quantum well energy (440 ± 35 nm) for different acceleration voltages. The scale bar is 2 µm long. (e) Normalized electron-hole pair generation probability in the active region simulated with CASINO. (inset) Schematic of the interaction volume at low (orange) and high acceleration voltage (green).

creases, allowing the generation of electron-hole pairs in the MQW from the top surface. Additional spectra for different acceleration voltages showing the optical contribution of each layer are available in section I of the supporting information (SI). However, this increase in penetration depth is accompanied by a decrease in spatial resolution. Indeed, by increasing the acceleration voltage from 10 kV to 20 kV, the CL spatial fluctuations become blurred (Figure 2 (c)-(d)).

To confirm these interpretations, we performed 3D Monte Carlo simulations[16] of the trajectories of the incident electrons near the sidewalls. Figure 2 (e) shows the normalized electron-hole pair generation probability in the active region for different acceleration voltages as a function of edge distance. These results suggest that the creation of electron-hole pairs depends on the geometry of the sample and the position of the electron beam. Thus, because of the change in excitation probability, the CL intensity does not necessarily capture the influence of surface recombination near the sidewalls but could also reflect local variations of injection or extraction efficiencies.

In order to be sensitive only to the local change of IQE, a more suitable approach is to probe the QW carrier lifetime itself.[17] Thus, we carried out SRTC-CL measurements to directly probe the carrier dynamics near the mesa edges.[18,19] As illustrated in Figure 3 (a), a Hanbury-Brown and Twiss interferometer is thus used to measure the CL photon autocorrelation function (g^2). Thanks to the specificity of the electron-matter interactions, g^2 measurements allow to retrieve the local carrier lifetime with the same spatial resolution as standard CL spectroscopy. In addition, the acceleration voltage is kept to 10 kV to efficiently probe the MQW region while having the best possible spatial resolution. The probe current has been set to 4 pA. More details on the SRTC-CL setup can be found in ref. 19.

We first investigated the carrier lifetime evolution across a single mesa. Figure 3 shows the SEM image (b) of a 3-µm large mesa together with its simultaneously acquired CL image (c). In analogy to time-resolved measurements, we display normalized autocorrelation functions for positive delays in Figure 3 (d). The corresponding scanning spots are color-coded and indicated in Figure 3 (b). To extract quantitative information, we then fitted the g^2 decays by a stretched exponential:

$$g^2(t) = 1 + g_0 \exp\left(-(|t|/\tau)^\gamma\right) \qquad (1)$$

where τ represents the average CL lifetime and

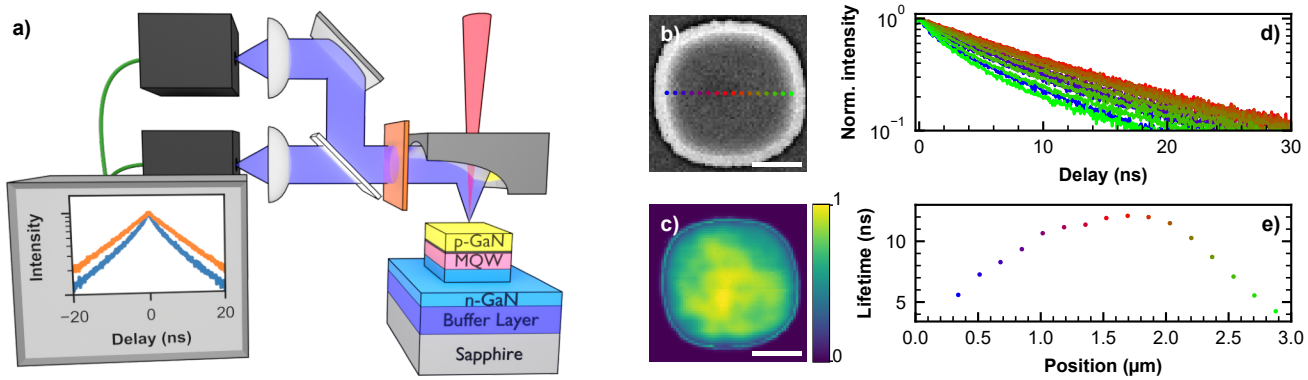

Figure 3: (a) Schematics of the SRTC-CL experimental setup. (b) SEM image of a 3-µm large mesa and (c) the corresponding CL image at MQW energy. The scale bar is 1-µm long. (d) Normalized g^2 for different positions on the mesa. (e) CL lifetime as a function of the position across the mesa.

γ is the stretching exponent.[20]

The CL lifetime across the mesa is displayed in Figure 3 (e). The CL lifetime is maximum in the center of the mesa where it reaches ≈ 12 ns. This value is kept on a plateau of $\approx$ 1 µm. As the electron beam approaches the sidewalls, the CL lifetime decreases over a characteristic length of $\approx$ 1 µm. Near the sidewalls, the carrier lifetime is less than 5 ns, highlighting the detrimental role of non-radiative surface recombinations, as it will be discussed in the following.

It should be noted, however, that the left and right edges do not seem to behave in the same way. The left edge appears to impact on a wider band the carrier lifetime. This effect can be linked to the inherent spatial fluctuations of CL intensity of MQWs (Figure 2 (c)). Indeed, even in the absence of any etching, the internal quantum efficiency of the active area can vary locally due to the presence of non-radiative centers such as dislocations or point defects (see SI section I.2 for a CL image at the center of a 2 $\times$ 2 mm^2 mesa presenting similar fluctuations). Due to the nanoscale resolution of SRTC-CL, this may locally modify the probed CL lifetime.

In order to average these fluctuations without compromising the spatial resolution, it is necessary to average the signal in the parallel direction to the sidewalls. Thus, instead of measuring the CL lifetime point by point, it is requested to integrate the CL signal parallel to an edge.

In view of an accurate analysis of non-radiative recombinations at an etched surface, we now focus our investigation on the center of a single edge of a 100-µm large mesa. Figure 4 shows a SEM image (a) with its simultaneously acquired CL image (b) near a sidewall. As discussed above, we noticed a local CL intensity enhancement when the e-beam is on the sidewall, due an increase of electron-hole pair generation in the active region. In addition, we observed the random spatial fluctuation in the mesa itself due to the presence of non-radiative defects. On Figure 4 (c), we thus average both the CL and the secondary electron (SE) signals in the transverse direction. As a result, intensity fluctuations are smoothed out and surface related effects are becoming more apparent. First, we observe that the maximum of the CL intensity is reached in the vicinity of the sidewall. More precisely, it matches a dip in the SE signal. This dip is assigned to the presence of the AlGaN EBL. As expected from our MC simulations, this corresponds to the situation where the overlap between the interaction volume and the active region is maximum. Even after averaging, the CL signal still shows some small fluctuations in intensity away from the edge but these are limited to ± 5 %. Finally, we observed that from a distance of about 450 nm from the edge, the CL signal decreases due to surface recombinations.

For SRTC-CL measurements, in order to maintain the spatial resolution while averaging along the transverse direction, we shaped the e-beam in a rectangle with a width of 100 nm

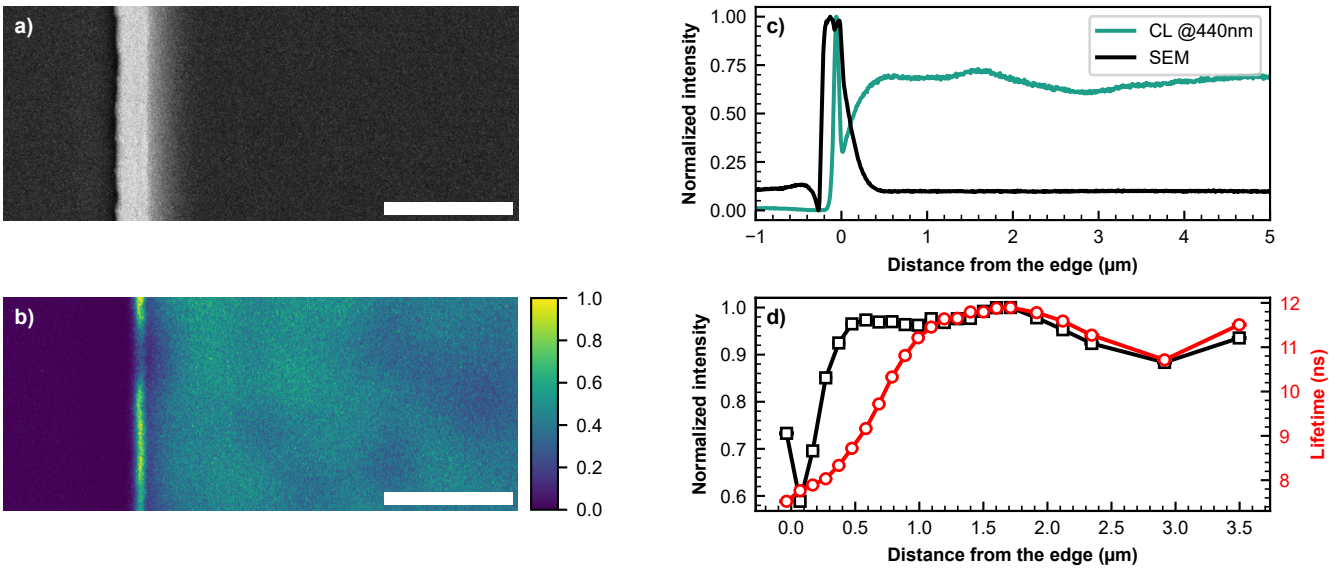

Figure 4: (a) SEM image near an edge of a 100-µm large mesa and (b) the corresponding CL image at MQW energy (440 ± 35 nm). The scale bar is 1-µm long. (c) SE and CL profiles averaged perpendicular to the edge. (d) Simultaneously acquired normalized CL intensity (black squares) and CL lifetime (red circles) as a function of the distance from the edge.

and a height of $\approx 7\,\mu$m. The normalized CL intensity and the CL lifetime are shown as a function of the distance from the edge on Figure 4 (d). First, we observe that the CL intensity recorded in the SRTC-CL setup is in excellent agreement with the results obtained on Figure 4 (c). Concerning the CL lifetime, two regimes can be identified. First, far from the edge, the variations of CL lifetime is correlated with CL intensity variations. In this region, both the CL lifetime and CL intensity reflect the local change in internal quantum efficiency. However, in a 1-µm band close to the etched surface, the situation is different. Indeed, between 450 nm and 1 µm from the edge, the CL lifetime decreases while the CL intensity remains almost unaffected. Only when the distance from the e-beam to the edge is less than 450 nm, the CL intensity decreases significantly.

Thus, it is clear that in the region of interest, i.e. near the surface, the CL intensity and CL lifetime do not carry the same information. To understand this, it is useful to clarify their relation with efficiencies :

$$I_{CL} \propto \eta_{inj} \times \eta_{IQE} \times \eta_{LEE} \tag{2}$$

$$\tau_{CL} = \eta_{IQE} \times \tau_{rad} \tag{3}$$

where η_{inj} is the injection efficiency, η_{IQE} the internal quantum efficiency, η_{LEE} the light extraction efficiency and τ_{rad} the radiative lifetime. From Equation 2, we can see that a change in CL intensity could be attributed to either a local change of η_{LEE}, η_{IQE} or η_{inj}. On the other hand, τ_{CL} only depends on η_{IQE} and τ_{rad}. Hence, the observed decrease of τ_{CL} could be linked to a reduction of radiative lifetime or IQE near the surface.

First, concerning the radiative lifetime, τ_{rad} could be affected by a local change in the internal electric field induced by the strain relaxation. To quantify this effect, we performed 6 x 6 k.p simulations, taking into account the strain relaxation and the electric field with nextnano3.[21] The parameters used for the simulations can be found in ref 22. We observed that the change in spatial electron-hole overlap is limited, with on average, a maximum variation of 20% within the first 200 nm from the edge depending on the QW (see SI Section II for more details). This cannot explain the trend followed by τ_{CL}. Thus, we conclude that the variation of τ_{CL} is mainly dominated by non-radiative re-

combinations at the sidewall surface. From the CL lifetime profile near the edge, it is clear that surface recombination plays a role up to 1 µm which already gives an estimation of the lateral diffusion length in the MQW region.

Therefore, if the IQE is decreasing near the sidewall, in order to explain the near constant CL intensity between 450 nm and 1.1 µm from the edge, either η_{inj} or η_{LEE} has to increase in this region. However, no local variation of η_{inj} is expected from our Monte-Carlo simulations (Figure 2 (e)). As a result, the different trend between CL lifetime and intensity in this region certainly arises from a local increase in light extraction efficiency. The origin of this increase could be explained by light scattering at the sidewalls,[13] increased sidewall emissions[23] or total internal reflections which could redirect the light at a more favorable angle for extraction.[8]

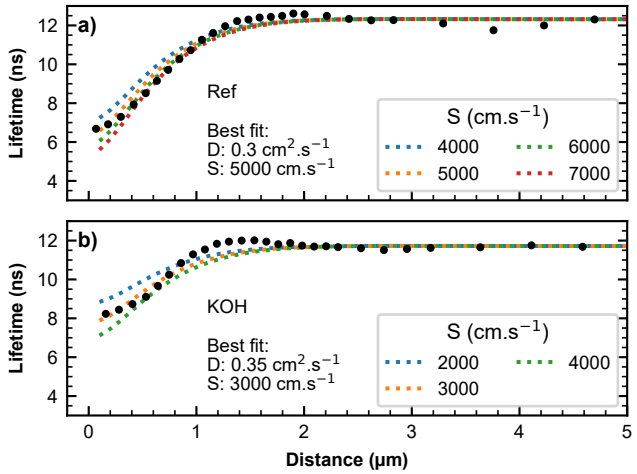

Figure 5: Lifetime profile of the untreated sample (a) and treated with KOH + Al_2O_3 (b) (black circle). 1D diffusion simulations for different surface recombination velocities are also shown as dotted line.

We then develop a 1D diffusion model taking into account non-radiative surface recombinations to extract quantitative information from our experimental results (see SI section III for more details). This model assumes a Gaussian electron beam characterized by a 150 nm standard deviation and a CL effective lifetime far from the edge of about 12 ns. Thus, the remaining fitting parameter are the diffusion coefficient D and the surface recombination velocity S. As observed in Figure 5 (a), the surface recombination velocity S mainly determines the magnitude of the near-surface lifetime while the diffusion coefficient D defines the lateral extension over which the surface plays a role (see SI section III). Thus, the parameters S and D are almost independent and can be adjusted separately, which ensures the robustness of the fit.

In order to validate our method and model, a room temperature KOH etching has been performed to reduced plasma damages followed by an Al_2O_3 deposition by atomic layer deposition.[8] As expected, we observed on Figure 5 (b) that the lifetime near the surface increases from 6 ns for the reference sample to 8 ns for the sample after KOH and Al_2O_3 treatment.

A statistical study has been then performed on 7 different sidewalls for both the reference and the treated samples. We then applied the fitting procedure to extract D and S (Table 1). As expected, we observed that only the surface recombination velocity changes from about 5.6×10^3 for the reference sample to about 3.1×10^3 cm s^{-1} for the sample after KOH and Al_2O_3 treatment while the diffusion coefficient remains around 0.33 cm^2 s^{-1}. These values are in line with previously published data obtained with other experimental techniques. Typical values of D can be found between 0.1 and 2 cm^2 s^{-1}.[24–26] S has been previously reported in the $[10^3$–$10^4]$ cm.s^{-1} range for etched III-nitride µLEDs.[27,28] From our results, we can

Table 1: Extracted model parameters for the reference sample (Ref) and passivated (KOH) sample. The uncertainty corresponds to one standard deviation.

	τ_{eff} (ns)	S (10^3 cm s^{-1})	D (cm^2 s^{-1})
Ref	11.8 ± 0.4	5.6 ± 1.4	0.33 ± 0.06
KOH	11.8 ± 0.3	3.1 ± 0.6	0.33 ± 0.06

draw some guidelines to the development of efficient µLEDs. First, in µLEDs with a diameter below 5 µm, non-radiative surface recombinations play an important role and cannot be neglected. However, from our model and experimental results, there are several direc-

tions to mitigate the detrimental role of the surface. First, starting with the most obvious, one way to improve the efficiency is to reduce the surface recombination itself by developing optimized surface treatments or implementing damage free etching techniques.[29] Then, another way to reduce the influence of the surface is to reduce the diffusion length, defines as $L \propto \sqrt{D\tau}$. Therefore, one can consider to decrease the diffusion coefficient D by engineering the potential fluctuation landscape.[30] Finally, the last option is to enhance the recombination rate. This could be achieved by reducing the QW thickness,[31] increasing the driving current[32] or by using semi-polar or non-polar structures. Additional simulations, showing the impact of these parameters on the IQE, are presented in SI Section III. Regarding all these aspects, core-shell microwire LEDs could also be an attractive solutions to produce efficient µLEDs with dimensions below 5 µm.

In conclusion, we studied the impact of etched sidewalls in µLEDs, which reduces the efficiency of InGaN/GaN QWs. We first demonstrate that CL intensity mapping can be affected by local changes in light extraction or injection efficiencies. Then, by combining SRTC-CL and a 1D diffusion model, we develop a methodology to quantitatively assess the precise role of surface recombinations. We finally demonstrate that the combination of KOH treatment and Al_2O_3 passivation layer drastically reduces surface recombinations.

Acknowledgement This work is supported by the French National Research Agency in the framework of the "Investissements d'avenir" program (ANR-15-IDEX-02) and with the help of the "Plateforme Technologique Amont" de Grenoble, with the financial support of CNRS Renatech network. The authors would like to thank Fabrice Donatini for his help in the development of the SRTC-CL setup.

Supporting Information Available

See Supporting Information section (I) for additional CL spectra for different acceleration voltages, (II) details of the nextnano simulations, (III) diffusion model and stretched exponential model and (IV) assessment of the CL excitation volume

References

(1) Olivier, F.; Daami, A.; Licitra, C.; Templier, F. Shockley-Read-Hall and Auger non-radiative recombination in GaN based LEDs: A size effect study. *Applied Physics Letters* **2017**, *111*, 022104.

(2) Tian, P.; McKendry, J. J. D.; Gong, Z.; Guilhabert, B.; Watson, I. M.; Gu, E.; Chen, Z.; Zhang, G.; Dawson, M. D. Size-dependent efficiency and efficiency droop of blue InGaN micro-light emitting diodes. *Applied Physics Letters* **2012**, *101*, 231110.

(3) Boroditsky, M.; Gontijo, I.; Jackson, M.; Vrijen, R.; Yablonovitch, E.; Krauss, T.; Cheng, C.-C.; Scherer, A.; Bhat, R.; Krames, M. Surface recombination measurements on III–V candidate materials for nanostructure light-emitting diodes. *Journal of Applied Physics* **2000**, *87*, 3497–3504.

(4) Choi, W. H.; You, G.; Abraham, M.; Yu, S.-Y.; Liu, J.; Wang, L.; Xu, J.; Mohney, S. E. Sidewall passivation for InGaN/GaN nanopillar light emitting diodes. *Journal of Applied Physics* **2014**, *116*, 013103.

(5) Wong, M. S.; Lee, C.; Myers, D. J.; Hwang, D.; Kearns, J. A.; Li, T.; Speck, J. S.; Nakamura, S.; Denbaars, S. P. Size-independent peak efficiency of III-nitride micro-light-emitting-diodes using chemical treatment and sidewall passivation. *Applied Physics Express* **2019**, *12*.

(6) Wong, M. S.; Hwang, D.; Alhassan, A. I.; Lee, C.; Ley, R.; Nakamura, S.; DenBaars, S. P. High efficiency of III-nitride micro-light-emitting diodes by sidewall passivation using atomic layer deposition. *Optics Express* **2018**, *26*, 21324.

(7) Otto, I.; Mounir, C.; Nirschl, A.; Pfeuffer, A.; Schäpers, T.; Schwarz, U. T.; von Malm, N. Micro-pixel light emitting diodes: Impact of the chip process on microscopic electro- and photoluminescence. *Applied Physics Letters* **2015**, *106*, 151108.

(8) Ley, R. T.; Smith, J. M.; Wong, M. S.; Margalith, T.; Nakamura, S.; DenBaars, S. P.; Gordon, M. J. Revealing the importance of light extraction efficiency in InGaN/GaN microLEDs via chemical treatment and dielectric passivation. *Applied Physics Letters* **2020**, *116*, 251104.

(9) Xie, E. Y.; Chen, Z. Z.; Edwards, P. R.; Gong, Z.; Liu, N. Y.; Tao, Y. B.; Zhang, Y. F.; Chen, Y. J.; Watson, I. M.; Gu, E.; Martin, R. W.; Zhang, G. Y.; Dawson, M. D. Strain relaxation in InGaN/GaN micro-pillars evidenced by high resolution cathodoluminescence hyperspectral imaging. *Journal of Applied Physics* **2012**, *112*, 013107.

(10) Boussadi, Y.; Rochat, N.; Barnes, J.-P.; Bakir, B. B.; Ferrandis, P.; Masenelli, B.; Licitra, C. Investigation of sidewall damage induced by reactive ion etching on AlGaInP MESA for micro-LED application. *Journal of Luminescence* **2021**, *234*, 117937.

(11) Olivier, F.; Daami, A.; Dupré, L.; Henry, F.; Aventurier, B.; Templier, F. 25-4: Investigation and Improvement of 10μm Pixel-pitch GaN-based Micro-LED Arrays with Very High Brightness. *SID Symposium Digest of Technical Papers* **2017**, *48*, 353–356.

(12) Jin, S. X.; Li, J.; Lin, J. Y.; Jiang, H. X. InGaN/GaN quantum well interconnected microdisk light emitting diodes. *Applied Physics Letters* **2000**, *77*, 3236–3238.

(13) Choi, H. W.; Jeon, C. W.; Dawson, M. D.; Edwards, P. R.; Martin, R. W.; Tripathy, S. Mechanism of enhanced light output efficiency in InGaN-based microlight emitting diodes. *Journal of Applied Physics* **2003**, *93*, 5978–5982.

(14) Meuret, S.; Coenen, T.; Woo, S. Y.; Ra, Y.-H.; Mi, Z.; Polman, A. Nanoscale Relative Emission Efficiency Mapping Using Cathodoluminescence g(2) Imaging. *Nano Letters* **2018**, *18*, 2288–2293.

(15) Reshchikov, M. A.; Morkoç, H. Luminescence properties of defects in GaN. *Journal of Applied Physics* **2005**, *97*, 061301.

(16) Demers, H.; Poirier-Demers, N.; Couture, A. R.; Joly, D.; Guilmain, M.; de Jonge, N.; Drouin, D. Three-dimensional electron microscopy simulation with the CASINO Monte Carlo software. *Scanning* **2011**, *33*, 135–146.

(17) Haller, C.; Carlin, J.-F.; Jacopin, G.; Liu, W.; Martin, D.; Butté, R.; Grandjean, N. GaN surface as the source of non-radiative defects in InGaN/GaN quantum wells. *Applied Physics Letters* **2018**, *113*, 111106.

(18) Meuret, S.; Tizei, L. H. G.; Auzelle, T.; Songmuang, R.; Daudin, B.; Gayral, B.; Kociak, M. Lifetime Measurements Well below the Optical Diffraction Limit. *ACS Photonics* **2016**, *3*, 1157–1163.

(19) Finot, S.; Grenier, V.; Zubialevich, V.; Bougerol, C.; Pampili, P.; Eymery, J.; Parbrook, P. J.; Durand, C.; Jacopin, G. Carrier dynamics near a crack in GaN microwires with AlGaN multiple quantum wells. *Applied Physics Letters* **2020**, *117*, 221105.

(20) Pophristic, M.; Long, F. H.; Tran, C. A.; Ferguson, I. T. Time-Resolved Photoluminescence Measurements of InGaN Light-

Emitting Diodes. *Materials Science Forum* **2000**, *338-342*, 1623–1626.

(21) Birner, S.; Zibold, T.; Andlauer, T.; Kubis, T.; Sabathil, M.; Trellakis, A.; Vogl, P. nextnano: General Purpose 3-D Simulations. *IEEE Transactions on Electron Devices* **2007**, *54*, 2137–2142.

(22) Vurgaftman, I.; Meyer, J. R. Band parameters for nitrogen-containing semiconductors. *Journal of Applied Physics* **2003**, *94*, 3675–3696.

(23) Ma, M.; Cho, J.; Schubert, E. F.; Park, Y.; Kim, G. B.; Sone, C. Strong light-extraction enhancement in GaInN light-emitting diodes patterned with TiO2 micro-pillars with tapered sidewalls. *Applied Physics Letters* **2012**, *101*, 141105.

(24) Jarašiūnas, K.; Aleksiejūnas, R.; Malinauskas, T.; Sūdžius, M.; Miasojedovas, S.; Juršėnas, S.; Žukauskas, A.; Gaska, R.; Zhang, J.; Shur, M. S.; Yang, J. W.; Kuokštis, E.; Khan, M. A. Carrier diffusion and recombination in highly excited InGaN/GaN heterostructures. *physica status solidi (a)* **2005**, *202*, 820–823.

(25) Solowan, H.-M.; Danhof, J.; Schwarz, U. T. Direct Observation of Charge Carrier Diffusion and Localization in an InGaN Multi Quantum Well. *Japanese Journal of Applied Physics* **2013**, *52*, 08JK07.

(26) Aleksiejūnas, R.; Gelžinytė, K.; Nargelas, S.; Jarašiūnas, K.; Vengris, M.; Armour, E. A.; Byrnes, D. P.; Arif, R. A.; Lee, S. M.; Papasouliotis, G. D. Diffusion-driven and excitation-dependent recombination rate in blue InGaN/GaN quantum well structures. *Applied Physics Letters* **2014**, *104*, 022114.

(27) Bulashevich, K. A.; Karpov, S. Y. Impact of surface recombination on efficiency of III-nitride light-emitting diodes. *physica status solidi (RRL) - Rapid Research Letters* **2016**, *10*, 480–484.

(28) Bulashevich, K.; Konoplev, S.; Karpov, S. Effect of Die Shape and Size on Performance of III-Nitride Micro-LEDs: A Modeling Study. *Photonics* **2018**, *5*, 41.

(29) Zhu, J.; Takahashi, T.; Ohori, D.; Endo, K.; Samukawa, S.; Shimizu, M.; Wang, X.-L. Near-Complete Elimination of Size-Dependent Efficiency Decrease in GaN Micro-Light-Emitting Diodes. *physica status solidi (a)* **2019**, *216*, 1900380.

(30) Shen, H.-T.; Weisbuch, C.; Speck, J. S.; Wu, Y.-R. Three-dimensional modeling of minority carrier lateral diffusion length in InGaN blue/green and AlGaN ultraviolet C single quantum wells including random alloy fluctuations. **2021**, 1–7.

(31) Weatherley, T. F. K.; Liu, W.; Osokin, V.; Alexander, D. T. L.; Taylor, R. A.; Carlin, J.-F.; Butté, R.; Grandjean, N. Imaging Nonradiative Point Defects Buried in Quantum Wells Using Cathodoluminescence. *Nano Letters* **2021**, *21*, 5217–5224.

(32) David, A. Long-Range Carrier Diffusion in (In,Ga)N Quantum Wells and Implications from Fundamentals to Devices. *Physical Review Applied* **2021**, *15*, 054015.

TOC Graphic

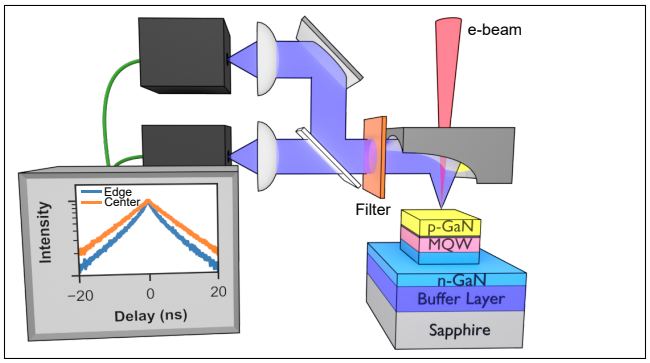
e-beam
Filter
p-GaN
MQW
n-GaN
Buffer Layer
Sapphire
Edge
Center
Intensity
−20
0
20
Delay (ns)